Electronic Supplementary Material (ESI) for Integrative Biology

Supplement – "**Quantifying cellular differentiation by physical phenotype using digital holographic microscopy" by K.J. Chalut, *et al*.**

Supplemental Methods

Cell culture and differentiation

HL-60 cells grow as single-cell suspension and require simple maintenance in vitro. Dr Donald E. Olins and Dr Ada L. Olins generously provided us with the HL-60/S4, a rapidly differentiating sub-line of HL-60 cells. This sub-line was cultured and induced to differentiate along the myeloid lineage following the procedure described in details elsewhere [1-4]. Briefly, HL-60/S4 cells were cultivated in RPMI 1640 medium supplemented with 2 mM L-Glutamine (Sigma R8758), with 10% heat inactivated FBS (GIBCO) and 1% penicillin/streptomycin (Invitrogen P4333) added. Cultures were propagated at 37°C under 5% CO_2 in 95% air, inside a humid incubator. The culture medium was sterile-filtered after preparation. Culture plates used were T-25 and T-75 flasks. A hemacytometer was used to judge the growth of the cells. Plateau was about $2x10^6$ cells/ml so culture density was maintained between $1x10^5$ cells/ml and $1x10^6$ cells/ml. Although HL-60 cultures can be maintained by diluting the cells with a fresh medium we found it better to re-passage rather than dilute in order to minimize debris in the medium (which interferes with trapped cells during OS measurements). Only cells in the logarithmic phase of growth were used for induction of differentiation. In this phase, viability was routinely above 98.5%, as determined using Trypan Blue dye (Invitrogen 15250-061).

All-trans retinoic acid (ATRA or RA), $C_{20}H_{28}O_2$, (Sigma R2625-50 mg) was used for generating neutrophils. 1-alpha, 25 Dihydroxyvitamin D3 (D3), $1,25(OH)_2D3$, (Sigma D1530-10µg) was used for inducing differentiation into monocytic cells and Phorbol 12-myristate-13-acetate (TPA or PMA), $C_{36}H_{56}O_8$, (Sigma, 79346) was for used generating macrophages. Chemical stock solutions were made as follows. RA at a concentration of 5 mM in ethanol: 50 mg was dissolved in 33.28 ml of 99.5% ethanol, kept in a 50 ml Falcon tube, wrapped in aluminum foil due to its photosensitivity and stored at -20^0C. D3 at a concentration of 100 µM in ethanol: 10 µg was dissolved in 2.4ml of 99.5% ethanol, kept in the manufacturer's rubber-sealed bottle, wrapped in aluminum foil due to its photosensitivity and stored at -20^0C. PMA at a concentration of 160 µM in acetone: 10.13 ml acetone was added to 1 mg PMA using a needle and syringe, kept in the manufacturer's tightly capped glass vessel and stored at -20^0C. Though photosensitivity was not indicated, it was treated as such by being wrapped in aluminum foil.

For differentiation into neutrophils, RA from stock solution was added to 1µM, that is, 25 µl of stock in 5 ml of cell culture medium. Cell density was rigorously kept at $1.5x10^5$ cell/ml after we found that the percentage of differentiated cells depended on cell density for all lineages. For differentiation into monocytic cells, D3 was added to 100 nM, that is, 5µl of D3 stock in 5 ml cell culture medium. Cell density was rigorously kept at $1.5x10^5$ cells/ml. For differentiation in macrophages, PMA was added to 16 nM, that is, 0.5 µl of PMA stock solution in 5 ml cell culture medium. Cell density was rigorously kept at $2.5x10^5$ cells/ml. During induced differentiation the T-25 and T-75 flasks were covered with aluminum foil to protect against light which would alter the concentrations.

Electronic Supplementary Material (ESI) for Integrative Biology

Digital holographic microscopy

The basic set up of the DHM is shown in Fig. S1. An off-axis hologram of a sample with intensity $I_H(x,y)$, is produced by the interference between the object wave, O(x,y), and the reference wave **R**(x,y) such that

$$I_H(x,y) = |\mathrm{R}|^2 + |\mathrm{O}|^2 + \mathrm{R}^*\mathrm{O} + \mathrm{R}\mathrm{O}^*.$$

The off-axis geometry allows the spectral separation of the phase terms (the third and fourth term) from the first two terms, which are DC terms. The third and fourth terms are carried to +1 and -1 diffraction order, and are therefore also separated in k-space (see Fig. 2b in manuscript). The offset angle, θ, in the off-axis geometry is governed by two factors: it must be large enough to separate the interference and DC terms in the Fourier transform, but must also be smaller than a maximum value θ_{max}, which is determined by the resolution of the detector

$$\theta_{max} = sin^{-1}\left(\frac{\lambda}{2\Delta p}\right) \approx \frac{\lambda}{2\Delta p}$$

where λ is the wavelength of the light beam and Δp is the pixel size. The value of θ is usually between one and three degrees.

The filter used to isolate one of the interference terms is a Gaussian filter, as this gives another Gaussian under Fourier transformation (Figure 4b), which does not have any high frequency components. The area inside the Gaussian is important: it must be small enough not to contain any of the zero order of diffraction, but large enough to avoid suppression of the high frequency components of the conjugate image term. Given a sufficiently large offset angle, however, the standard deviation of the Gaussian is easily chosen so that the low-pass filtering effect is negligible. The phase information of the sample can finally be extracted from the isolated conjugate image:

$$\varphi(x,y) = tan^{-1}\left(\frac{Im(x,y)}{Re(x,y)}\right)$$

where φ is the wrapped phase and *Re* and *Im* are the real and imaginary parts of the wave respectively. φ is defined as the wrapped phase because, due to the periodicity of the tangent function, it is constrained to lie between $-\pi$ and π and is therefore not continuous. The phase can be unwrapped by adding multiples of 2π whenever φ experiences a large jump in value. This generates the qualitative phase image. The refractive index is extracted as described in the manuscript. Thorough exploration of the use of off-axis DHM for biological imaging can be found in many of the references from the group of Christian Depeursinge, for example [5-7]. There has also been other important work on understanding the DHM modality for biological imaging in the group of Adam Wax [8, 9], Gert von Bally [10], and others referenced in the manuscript.

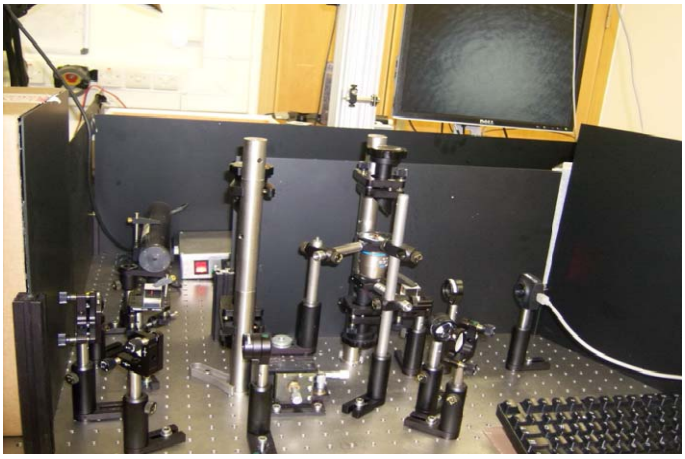

Fig. S1 DHM set up. The DHM is a laser-based table-top setup that uses a microscope objective and a reference arm, therefore enabling an interferometric system to analyze the quantitative phase of biological samples.

Sample preparation, DHM imaging and analyses

Cells in culture medium were placed on microscope slides coated with poly-D-lysine and incubated for 10 minutes to allow them stick on the slides while maintaining their near-spherical shape, washed with phosphate-buffered saline (PBS) and placed on the inverted microscope objective for imaging. The hologram is acquired at the video frequency of a CCD or CMOS camera. Fig. S5 illustrates image analysis steps.

To deduce the refractive index distributions from DHM, we assumed sphericity of the cells, and thereby the thickness for each line of sight in the cell. Sphericity was verified for each cell. We also measured a sample of suspended cells, as opposed to the technique presented in this paper in which cells were adhered with PDL to microscope slides, and deduced the same average refractive index with each method. Additionally, because of slight deviations from sphericity at the edges (due to deformations in the membrane itself) we avoided the edges by analyzing the inner 85% by radius of each cell. This has the additional advantage of putting an emphasis on the nuclear contribution to the refractive index distribution.

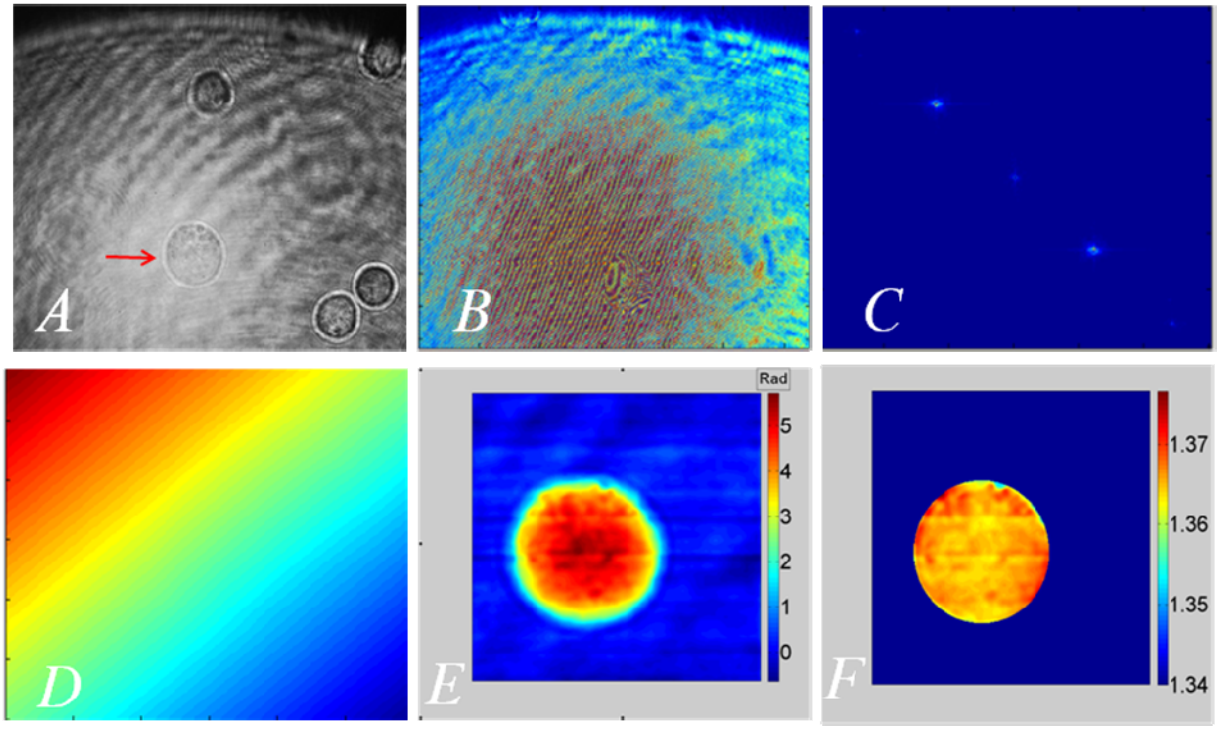

Fig. S2 Image processing stages. (*A*): An off-axis hologram of cells (see red arrow for cell analyzed); (*B*): zero-padding of image removed; (*C*): 2-D shifted Fourier Transform; (*D*): unwrapped phase image; (*E*): quantitative phase image of arrowed cell; (*F*): refractive index distribution of the cell from which an average, n_avg, is determined. (*B*)-(*F*) were achieved using codes in MATLAB and C. Detailed principles behind direct hologram recording by a CCD target and numerical reconstruction are found in[11].

Measurement of compliance by optical stretching

In using the OS, cells are first trapped at low powers and then stretched at higher powers. Although various stress patterns are possible as input, we used a step stress pattern which, by rheological definition, gives a strain output that can be converted to a material property called creep compliance. Each cell was held in the trap for 2 s, at a power of 0.2 W per fibre, stretched for 4 s at 1.5 W per fibre and allowed to relax at the trapping power for 4 s. The OS is operated by computer controls using an in-house developed LabVIEW program. The edges of cells on images of stretched cells were detected and then fitted to ellipses using other custom-made LabVIEW programs. The final output gives the relative deformation of each cell expressed as a percentage and defined as the relative major axial extension or strain of each cell as a function of time, γ(t). Thus,

$$time-dependent\ deformation\ \ \gamma(t)=\frac{a(t)-a_o}{a_o}\,\mathrm{x}\,100, \qquad (1)$$

where $a(t)$ is the semi-major axis aligned with the beam axis of the fit ellipse and a_0 is the average of the values of $a(t)$ during the 2 s when the cell is trapped before stretching. The tensile compliance, $D(t)$, is obtained thus:

$$tensile\ creep\ compliance\ \ D(t)=\frac{\gamma(t)}{100*\sigma_o F_g}, \qquad (2)$$

where F_g is a geometric factor which accounts for the shape of the cell in the OS [12] and σ_o is a constant value of the applied stresses calculated using an analytic-numerical model based on electromagnetic wave optics [13, 14]. This modeling approach to determining optical stresses applied in the OS is necessitated by the absence of a direct method of measuring the optical stress. Also for the calculation of compliance, the refractive indices of the cells are required. The refractive indices of cells can be measured using the index matching/phase contrast method [15]. In order to separate the optical properties of differentiating cells from the mechanical properties, we used DHM to monitor and estimate the average refractive index of cells at the same time points as compliance measurements.

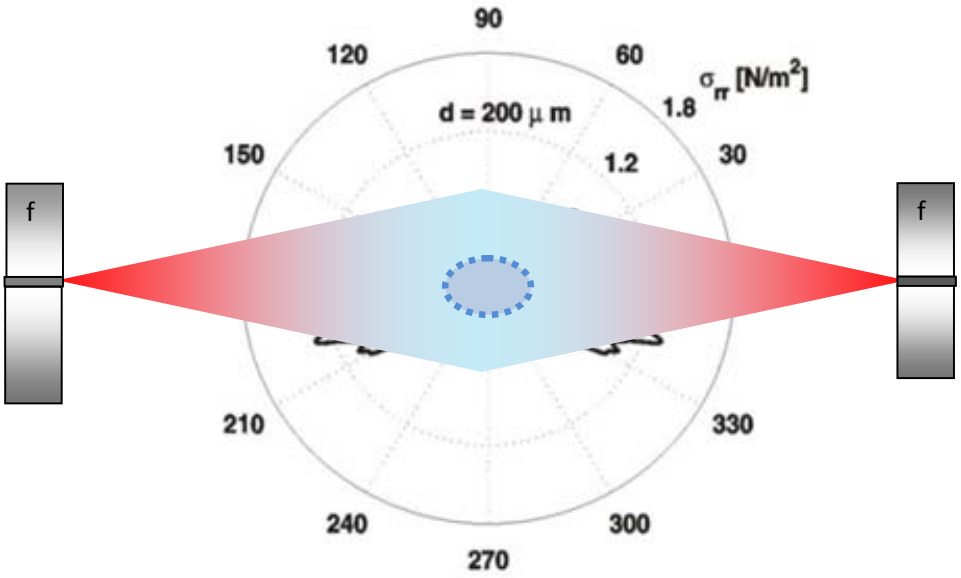

Figure S3 Physical principle of an optical stretcher. Two-counter propagating and diverging near infra red laser beams (λ = 1064 nm) in Gaussian profile emanating from the cores of single-mode optical fibers (f) are used to trap (at 0.2 W per fibre) and deform (at 1.5 W per fibre) single cells. The forces that deform the cell along the surface arise from the change in the refractive index at cell-medium interface and the ensuing conservation of momentum. Radial optical pressure (σ_{rr}) represented by graphed black line on the trapped cell (solid blue line) and stretched cell (broken blue line) is computed using an electromagnetic wave model (see [14]) which gives stress profiles with interference-smoothened spikes.

Confocal imaging of HP1α distributions

The cells were attached to microscope slides using poly-D-lysine and then fixed using either 4% paraformaldehyde or methanol. For each fixation, two samples for each differentiation routine at each time point were prepared, and each fixation technique was tried twice total to ensure reproducibility. Primary antibody against HP1α (clone 15.19s2 Millipore, USA) was used at a dilution 1:200 in the presence of 0.1% Triton X-100 for 2 h. The nuclei were stained with the secondary goat anti-mouse alexa-633 (Invitrogen/Molecular Probes) for 1h. hMSCs were washed twice in PBS and mounted using gel mount (Biomeda, Foster City, CA). Confocal images were taken on a Leica SP5 inverted confocal microscope using a 63x oil-immersion objective. Fractal dimension was found using the FracLac plugin for ImageJ. For measuring nuclear to cytoplasmic ratio, live cells were double stained with one

dye for nuclei (SYTO 61, Invitrogen, 775304) and another dye for cytoplasm including mitochondria (MitoTracker Orange CMTMRos, Invitrogen, 815301). After incubation in culture media with the two dyes each at a final concentration of 10 μM for 1 hour, cells were centrifuged, resuspended in culture media, incubated for 10 mins, washed again in culture media, placed on a depression slide and brought to a Leica SP5 inverted confocal microscope where confocal images were taken using a 63x oil-immersion objective. In-house code was developed in Matlab (Mathworks, Natwick, MA), for simultaneous segmentation of the nucleus and the cytoplasm in cross-sectional images of single cells.

Statistical methods

A ranksum test ($\alpha = 0.05$) was used in Matlab to test for statistical significance and reproducibility.

Supplemental Results

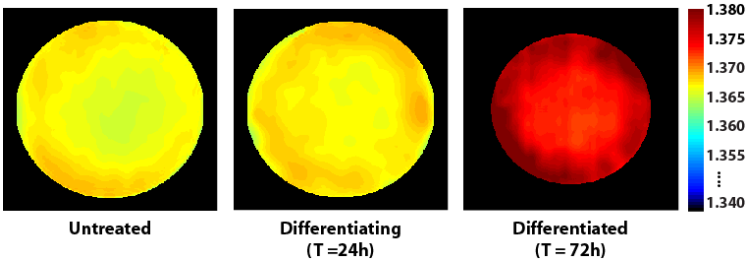

Fig. S4 Average RI distributions of macrophage differentiation using DHM.

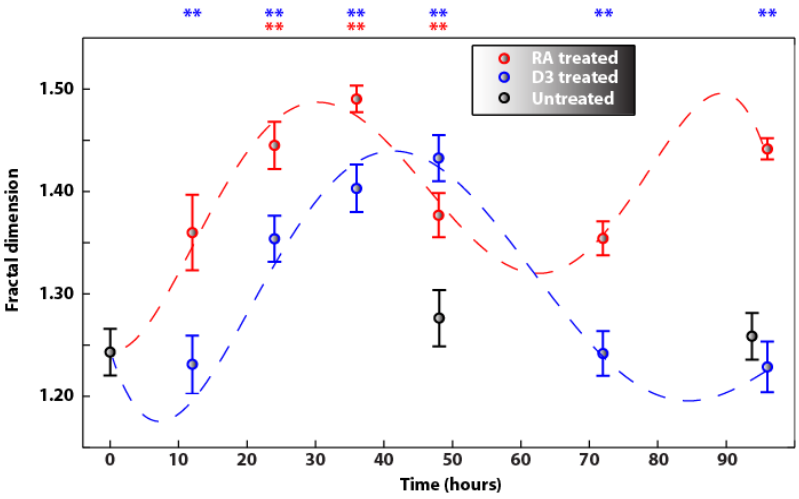

Fig. S5 Fractal dimension of HP1α distributions during neutrophil and monocyte differentiation. A larger fractal dimension indicates a greater uniformity in the distribution; therefore, a change from a smaller to a larger fractal dimension indicates that the HP1α protein is diffusing through the nucleus. The subsequent increase in fractal dimension observed in neutrophil differentiation is almost certainly due to changes in subnuclear structure due to nuclear lobulation.

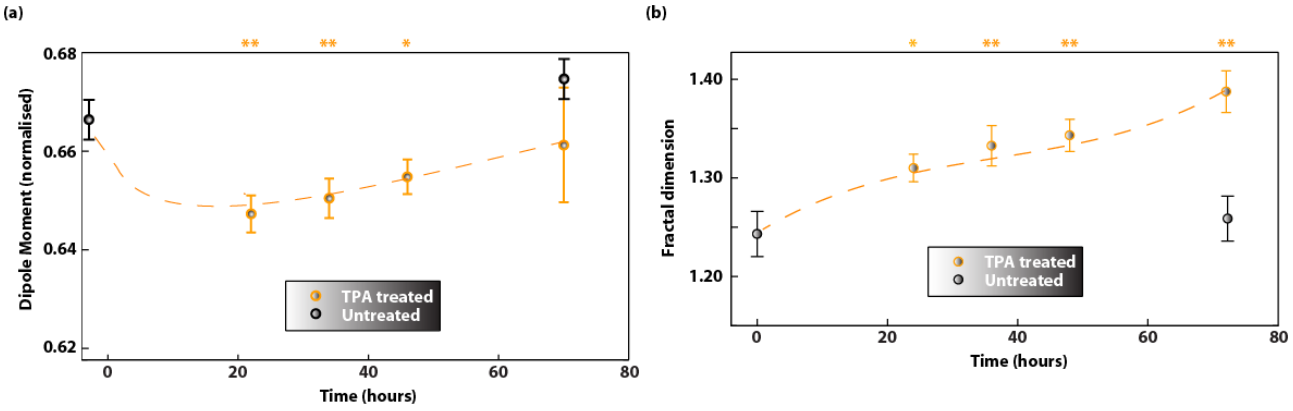

Fig. S6 Changes in dipole moment (a) and fractal dimension (b) of HP1α distributions during macrophage differentiation.

References

[1] A. L. Olins *et al.*, Experimental Cell Research **245**, 91 (1998).
[2] A. L. Olins *et al.*, Experimental Cell Research **268**, 115 (2001).
[3] A. L. Olins *et al.*, European Journal of Cell Biology **88**, 203 (2009).
[4] A. L. Olins *et al.*, Experimental Cell Research **254**, 130 (2000).
[5] E. Cuche, F. Bevilacqua, and C. Depeursinge, Optics letters **24**, 291 (1999).
[6] E. Cuche, P. Marquet, and C. Depeursinge, Applied optics **39**, 4070 (2000).
[7] P. Marquet *et al.*, Optics letters **30**, 468 (2005).
[8] N. T. Shaked, M. T. Rinehart, and A. Wax, Optics letters **34**, 767 (2009).
[9] N. T. Shaked *et al.*, Optics express **17**, 15585 (2009).
[10] B. Kemper, and G. von Bally, Applied optics **47**, A52 (2008).
[11] U. Schnars, and W. Jüptner, Appl. Opt. **33**, 179 (1994).
[12] F. Wottawah *et al.*, Acta Biomaterialia **1**, 263 (2005).
[13] J. Guck *et al.*, Biophysical Journal **88**, 3689 (2005).
[14] L. Boyde, K. J. Chalut, and J. Guck, J. Opt. Soc. Am. A **26**, 1814 (2009).
[15] R. Barer, K. F. A. Ross, and S. Tkaczyk, Nature **171**, 720 (1953).